Analytical Biochemistry 447 (2014) 90–97

Contents lists available at ScienceDirect

Analytical Biochemistry

journal homepage: www.elsevier.com/locate/yabio

Intravital imaging of *Bacillus thuringiensis* Cry1A toxin binding sites in the midgut of silkworm

Na Li [a,b], Jing Wang [a,b], Heyou Han [a,b,*], Liang Huang [a], Feng Shao [a], Xuepu Li [a]

[a] State Key Laboratory of Agricultural Microbiology, College of Science, Huazhong Agricultural University, Wuhan 430070, People's Republic of China
[b] College of Food Science & Technology, Huazhong Agricultural University, Wuhan 430070, People's Republic of China

ARTICLE INFO

Article history:
Received 15 August 2013
Received in revised form 25 October 2013
Accepted 7 November 2013
Available online 16 November 2013

Keywords:
Quantum dots
Cry1A toxins
In vivo imaging
Binding sites

ABSTRACT

Identification of the resistance mechanism of insects against *Bacillus thuringiensis* Cry1A toxin is becoming an increasingly challenging task. This fact highlights the need for establishing new methods to further explore the molecular interactions of Cry1A toxin with insects and the receptor-binding region of Cry1A toxins for their wider application as biopesticides and a gene source for gene-modified crops. In this contribution, a quantum dot-based near-infrared fluorescence imaging method has been applied for direct dynamic tracking of the specific binding of Cry1A toxins, CrylAa and CrylAc, to the midgut tissue of silkworm. The in vitro fluorescence imaging displayed the higher binding specificity of CrylAa–QD probes compared to CrylAc–QD to the brush border membrane vesicles of midgut from silkworm. The *in vivo* imaging demonstrated that more CrylAa–QDs binding to silkworm midgut could be effectively and distinctly monitored in living silkworms. Furthermore, frozen section analysis clearly indicated the broader receptor-binding region of Cry1Aa compared to that of Cry1Ac in the midgut part. These observations suggest that the insecticidal activity of Cry toxins may depend on the receptor-binding sites, and this scatheless and visual near-infrared fluorescence imaging could provide a new avenue to study the resistance mechanism to maintain the insecticidal activity of *B. thuringiensis* toxins.

Biopesticides are one of the most important tools for establishing an integrated pest management program, which is seen as a significant factor in promoting sustainable agriculture. Various *Bacillus thuringiensis* (Bt) formulations have been widely used as biopesticides, and genetically modified crops carrying Cry genes have been developed [1,2]. Bt, a gram-positive bacterium, produces many kinds of insecticidal crystal proteins [3], including Cry1A, Cry1B, Cry1C, and so on. Cry toxins are expressed in inclusion bodies as protoxins (70 to 140 kDa) during sporulation. The crystal protoxins ingested by target insects are dissolved in the highly alkaline gut juice and activated by proteases. After enzymatic activation, the toxic protease-resistant fragment, which is the 60- to 65-kDa activated toxin, binds to specific receptors located in the midgut tissue of host insects to cause the insect's death [4–7]. However, the widespread adoption of Bt biopesticides and transgenic crops has increased the evolution of resistance by pests and poses threats to the continued success of Bt biopesticides and crops [8–10]. To continue use of the environmentally friendly biopesticide, it is of great concern to clearly understand the binding of the activated Bt toxin to a specific midgut receptor, which is a key factor for insecticidal activity. Therefore, to understand what actually determines insecticidal activity, it is necessary to establish a new analytical method for the binding process of Cry1A toxin to the insect midgut tissue. The silkworm is sensitive to Cry1Aa and Cry1Ac, and compared to other Lepidoptera insects, the midgut of silkworm is easier to extract [11,12]. The receptors and the molecular mode of action of Cry1A have also been studied in silkworm by Sato's laboratory [13–16]. Thus, silkworm was selected as a model insect to evaluate and validate the detection method for the binding sites. Even though there are reports that Cry1Aa is more highly insecticidal than Cry1Ac, it is still unsure whether the loss of insecticidal activity is derived from a reduction in the receptor-binding sites [5,10,17–20]. Hence it is very necessary to conduct more detailed research in the receptor-binding region to provide a reliable explanation of the different insecticidal activities between Cry1Aa and Cry1Ac.

The current research methods concerning Bt toxin binding to midgut tissue include ligand and Western blot analyses, surface plasmon resonance, radioiodination, and so on [21–25]. These analytical methods for the interactions between Cry toxin and insects have been conducted with in vitro systems, such as cultured cells and tissues. However, it is very difficult to acquire information as close as possible to intact binding, because the extraction by detergent is very artificial and various proteins that are involved in the

* Corresponding author at: State Key Laboratory of Agricultural Microbiology, College of Science, Huazhong Agricultural University, Wuhan 430070, People's Republic of China. Fax: +86 27 87288246.
E-mail address: hyhan@mail.hzau.edu.cn (H. Han).

0003-2697/$ - see front matter © 2013 Elsevier Inc. All rights reserved.
http://dx.doi.org/10.1016/j.ab.2013.11.011

toxin binding region may lose their integrity [21]. Therefore, to avoid these drawbacks, it is highly desirable to exploit direct, scatheless, and visualized diagnoses for dynamically monitoring the complete course of the Cry1Aa and Cry1Ac toxins binding to their *in vivo* targets.

Near-infrared (NIR) fluorescence imaging has attracted intense attention because of its minimized biological autofluorescence background and the increased penetration of excitation and emission light through tissues in the NIR wavelength window (650–900 nm) [26,27]. Quantum dots (QDs) hold great promise as NIR material and are attracting more and more attention for their potential application in cell imaging and *in vivo* animal targeting [28]. He et al. [29] initially used water-dispersed NIR QDs for real-time *in vivo* tumor targeting. Recently, our research group successfully applied folic-acid-functionalized NIR QDs for visually active-targeting tumor *in vivo* [27]. The high-resolution images of the real-time and dynamic tumor targeting *in vivo* could be observed clearly. Therefore, NIR fluorescence imaging in living silkworm is proposed as a new method for real-time and dynamical tracking of Cry1Aa and Cry1Ac toxin binding.

The purpose of this paper is to report a NIR fluorescence imaging-based method for investigating the Cry1Aa- and Cry1Ac-specific binding and dynamic targeting in living silkworms in real time. The principle of our work is schematically represented in Fig. 1. First, we prepared the Cry1A–QD probes using a 1-ethyl-3-(3-dimethylaminopropyl)carbodiimide hydrochloride (EDC) and *N*-hydroxysulfosuccinimide sodium salt (sulfo-NHS) conjugation strategy and implemented characterizations for the conjugation. Then, the prepared NIR probes were used for both *in vitro* and *in vivo* imaging. We investigated the specific binding and targeting ability of prepared probes *in vivo*. Finally, it is worth mentioning that the fluorescence imaging of frozen sections reflected the distribution of binding sites of Cry1Aa and Cry1Ac. It is considered that NIR fluorescence imaging could provide information for further study of the mechanism of Cry toxin action in detail and a more precise mechanism of pest resistance.

Materials and methods

Materials

The silkworm eggs were purchased from Shandong Guangtong Silkworm Holdings Ltd. The Bt toxic proteins Cry1Aa and Cry1Ac were purchased from Envirologix. 4-(2-Aminoethyl)benzenesulfonyl fluoride hydrochloride (AEBSF), mannitol, and ethylene glycol bis(2-aminoethyl) tetraacetic acid (EGTA) were all purchased from Sigma. EDC and sulfo-NHS were purchased from Sigma. 3-(4,5-Dimethylthiazol-2-yl)-2,5-diphenyl tetrazolium bromide (MTT) was purchased from Aldrich. Cells were obtained from the State Key Laboratory of Agricultural Microbiology. All chemicals concerned were of analytical grade or the highest purity available and used without further purification. In addition, ultrapure water

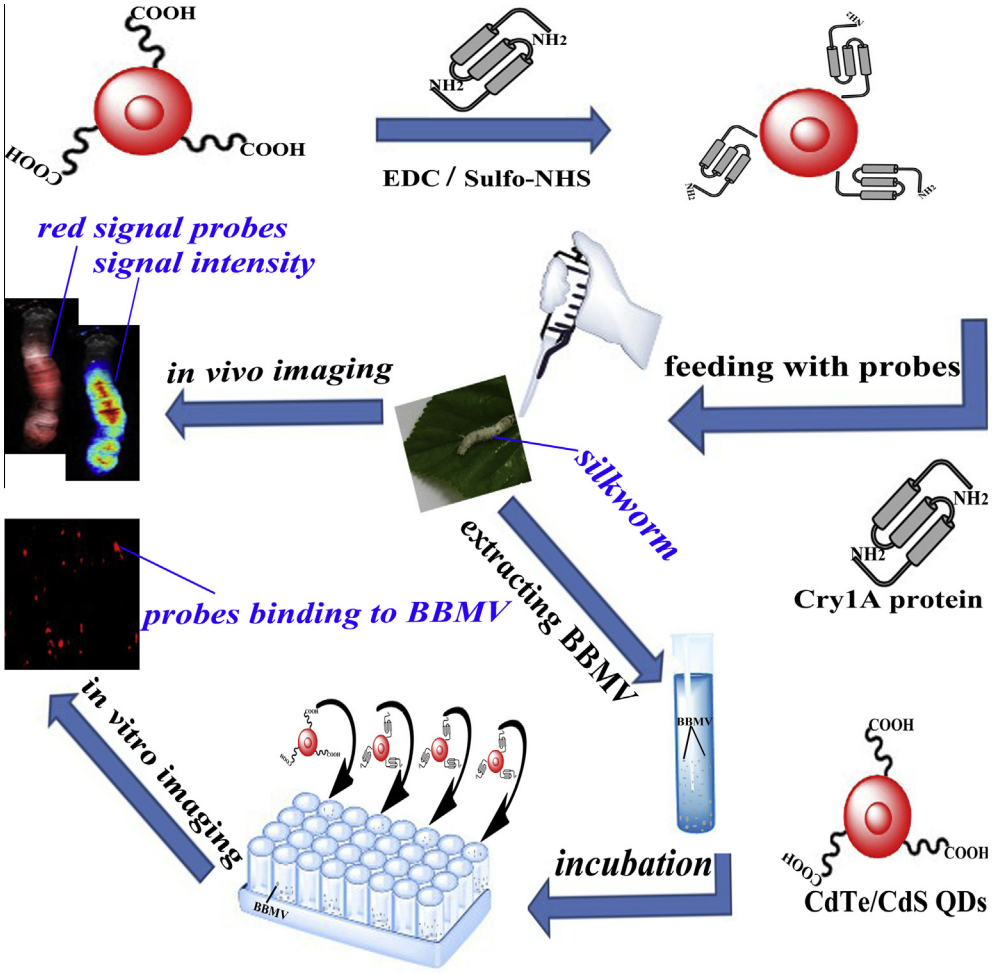

Fig.1. Schematic illustration of the QDs functionalized with Cry1A protein for visually active-targeting silkworm in vivo.

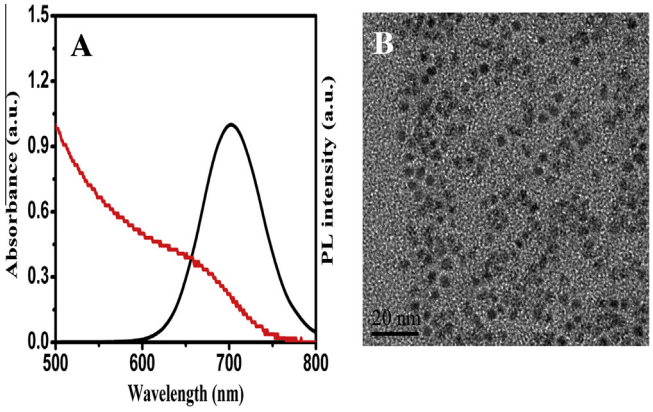

Fig.2. The characterization of the prepared NIR CdTe/CdS $core_{small}/shell_{thick}$ QDs. (A) The UV–Vis absorption spectra and PL spectra. (B) TEM image of NIR CdTe/CdS $core_{small}/shell_{thick}$ QDs.

(Millipore) with a conductivity of 18 MΩ cm was used throughout the experiments.

Instrumentation

Photoluminescence (PL) spectra and photostability of QDs were performed on an FLS920 spectrometer (Edinburgh, UK). The nanoparticle diameters were determined by dynamic light scattering (DLS) with a Zetasizer Nano ZS nanoparticle size analyzer (Malvern Instruments, UK). Transmission electron microscopy (TEM) images were obtained using a JEM-2010FEF microscope (JEOL, Japan). Agarose gel electrophoresis (AGE) was performed on a Beijing 61 DYY-6C electrophoresis unit (Beijing, China). Fluorescence images were recorded with a Nikon inverted CMS DM-4000M fluorescence microscope (Nikon, Japan). *In vivo* images of the silkworms were acquired using a CRi-Maestro2 *in vivo* imaging systems (PerkinElmer, USA). Frozen sections were prepared using a Thermo Scientific Cryotome E freezing microtome (Thermo Scientific, USA).

Incubation of silkworms

The purchased silkworm eggs were stored in the refrigerator at 4 °C. A moderate amount of silkworm eggs were taken out and these silkworm eggs were incubated at 25 °C. About 2 weeks after inoculation, the hatched larvae were fed with fresh mulberry leaves. When grown to various age stages, the silkworms were used for the following experiments.

Preparation of NIR CdTe/CdS $core_{small}/shell_{thick}$ QDs

MPA-capped NIR CdTe/CdS $core_{small}/shell_{thick}$ QDs were directly prepared in aqueous solution according to the previously published literature [30]. In brief, under an atmosphere of nitrogen, 0.0571 g of $CdCl_2{\cdot}2.5H_2O$ was dissolved in 50 ml of water, and

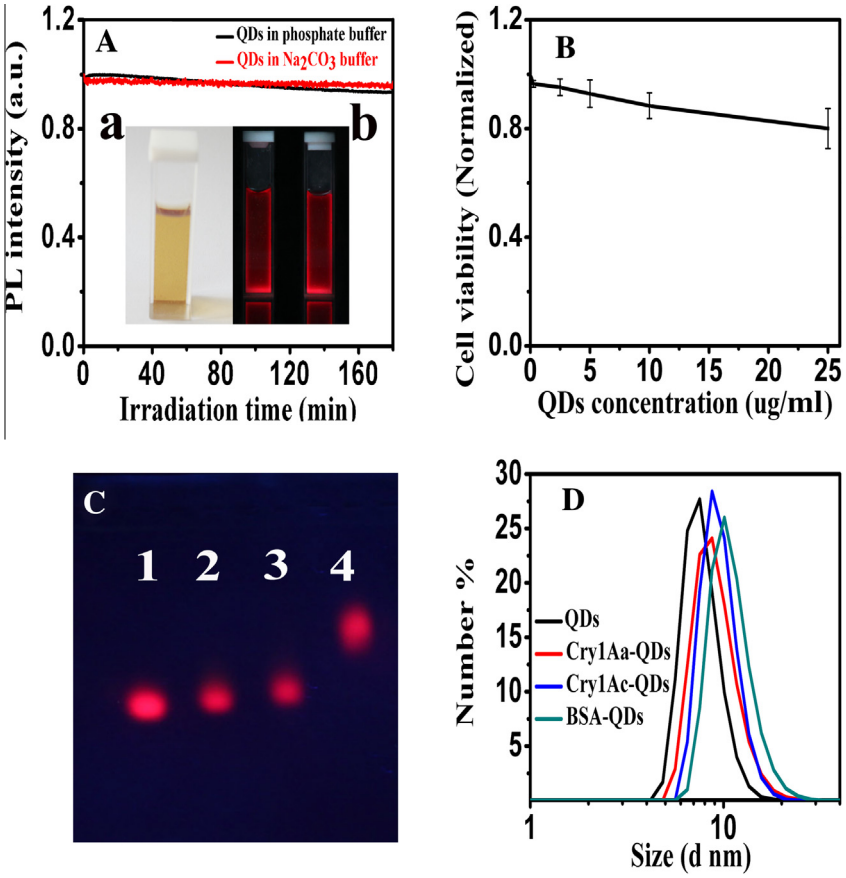

Fig.3. (A) The photostability of the CdTe/CdS QDs in Na_2CO_3 buffer (pH 10.0) solution and PBS (pH 7.4). Inset: (a) bright-field image and (b) fluorescence image of the CdTe/CdS QD solution placed in a 4 °C refrigerator for more than 3 months. (B) Cytotoxicity of QDs at various concentrations after incubation with HeLa cells. The cell viability was calculated by normalizing to the viability of the control (untreated) cells. The viability of the control cells was considered to be 1.0. The error bars represent the standard deviation of three measurements. (C and D) Characterization of conjugates. (C) AGE electrophoresis (the gel was run for 50 min at a constant voltage of 80 V at room temperature; 1% agarose gel, 0.5× Tris/borate running buffer) of QDs and conjugates: lanes 1, QDs; 2, Cry1Aa–QD conjugates; 3, Cry1Ac–QD conjugates; 4, BSA–QD conjugates. (D) Dynamic light scattering graphs for QDs and conjugates in Na_2CO_3 buffer (pH 10.0) solution.

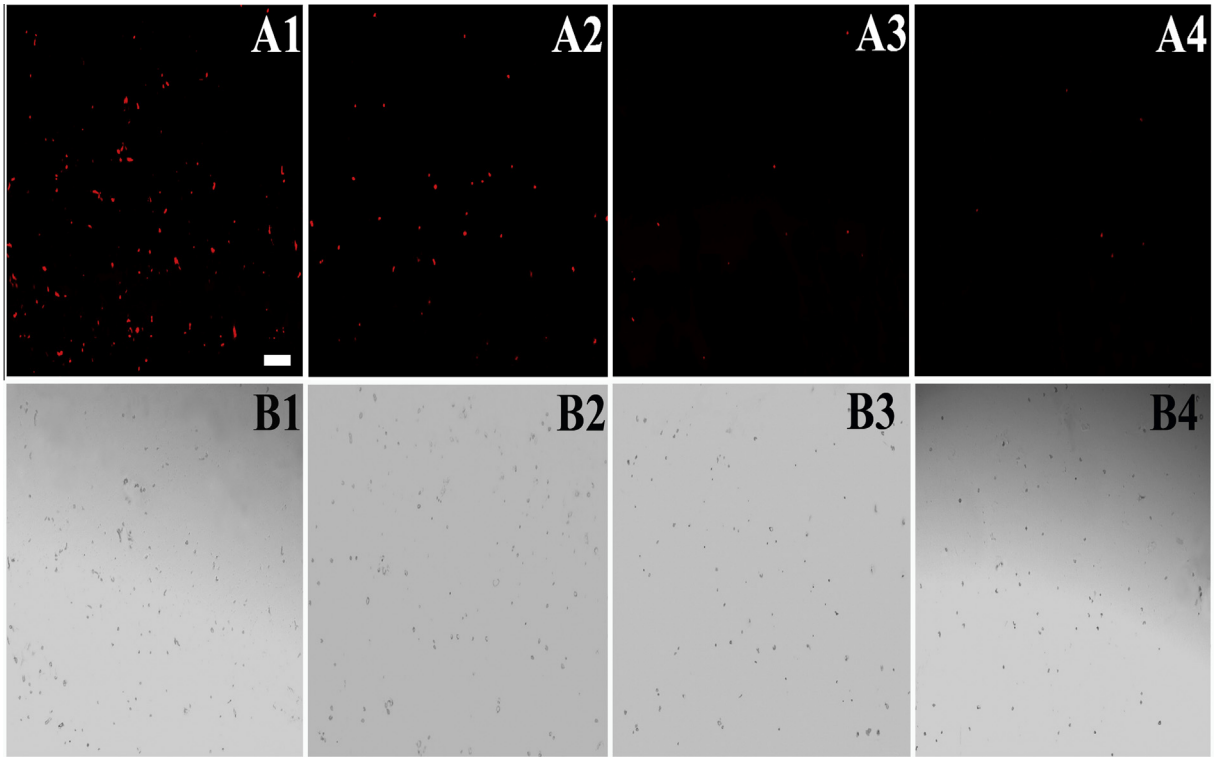

Fig.4. Microscopic images of BBMVs treated with QD-labeled (1) Cry1Aa, (2) Cry1Ac, (3) BSA, and (4) QDs. The upper images (A1–A4) show the fluorescence images of the BBMVs and the lower images (B1–B4) show the optical images of the BBMVs. Bar, 100 μm.

37 μl of MPA was added under stirring, followed by adjusting the pH to 12 by adding 1.0 M NaOH dropwise. Then, the freshly prepared 2 ml of NaHTe solution (2.0×10^{-5} mol) was injected into the above solution. Afterward, the solution was aged at 4 °C overnight and the small CdTe cluster solution was obtained. The NIR CdTe/CdS $core_{small}/shell_{thick}$ QDs were synthesized by further aging the small CdTe cluster solution at 90 °C for 8 h. The final concentration of the purified QDs was about 0.5 mg/ml and they were stored in a refrigerator at 4 °C.

MTT assay of cell viability

The MTT assay was carried out following a previously published method [31]. After cells were treated in the absence or presence of varying concentrations of CdTe/CdS QDs (0.25 to 25 μg/ml), the culture medium was removed and replaced with fresh medium (100 μl/well) and 20 μl/well MTT stock, followed by incubation for 4 h at 37 °C. The medium was removed and the remaining attached cells were rinsed with phosphate-buffered saline (PBS; 100 μl/well), then the cells were lysed and formazan was dissolved in dimethyl sulfoxide (100 μl/well). Absorbance was measured at 570 nm using an enzyme-linked immunosorbent detector. All measurements were done in duplicate in three independent experiments. To obtain complementary evidence, the biochemical assays of viability were confirmed via bright-field microscopy.

Conjugation of Bt toxin proteins with NIR QDs

First, 1 ml of 0.5 mg/ml QD solution was mixed with 50 μl of 50 mM EDC and 50 μl of 25 mM sulfo-NHS in PBS solution (pH 7.4). After 30 min of magnetic stirring, 1 ml of Cry1Aa (0.5 mg/ml solution in Na_2CO_3 buffer) was added to the reactor bottle and stirred at room temperature for another 4 h and then kept overnight in the refrigerator at 4 °C. A similar procedure using Cry1Ac or bovine serum albumin (BSA) instead of Cry1Aa was applied to the synthesis of Cry1Ac–QD or BSA–QD conjugates. After the coupling, the unreacted material was removed by ultrafiltration using a 50-kDa filter and three washes to obtain the Cry1Aa–QD, Cry1Ac–QD, and BSA–QD conjugates. The resultant conjugates were redispersed in Na_2CO_3 buffer (pH 10.0) to a final volume of 1 ml and stored at 4 °C for further use.

Preparation of the brush border membrane vesicles (BBMVs)

BBMVs from the midgut of fifth-instar silkworm larvae were prepared according to the method described by Wolfersberger et al. [32,33]. A total of 20 fifth-instar silkworm larvae were dissected behind the head and near the rear end. The midgut was pulled out of the dissected body and rinsed in 0.15 M normal saline. The midguts mixed with liquid nitrogen were ground rapidly in a ceramic mortar. The midgut homogenate was dispersed in a volume of 2 ml (0.1 ml for each midgut) prechilled BBMV buffer (0.3 M mannitol/5 mM EGTA/50 mM Tris–HCl, pH 8.0; 1 mM AEBSF). An equal volume of cold 24 mM $MgCl_2$ was added, and the mixture was incubated on ice for about 15 min and then centrifuged for 15 min at 4 °C (4800 rpm). The collected supernatant was centrifuged again for about 50 min at 4 °C (13,000 rpm). After centrifugation, the supernatant was removed and the centrifuge tube was inverted on ice for 15 min. Then the prepared BBMVs were washed three times with PBS (pH 7.4, containing 0.13 M NaCl and 2.7 mM KCl) for 10 min each and were resuspended in PBS and finally were stored at 4 °C.

Fluorescence microscopy of BBMVs interacting with QDs, Cry1Aa–QDs, Cry1Ac–QDs, and BSA–QDs

For specific binding studies, 100 μl of the BBMVs was incubated individually with 20 μl each of QDs, Cry1Aa–QD, Cry1Ac–QD, or BSA–QD conjugates in PBS for 2 h at 4 °C and then washed with PBS three times for 10 min each. Finally, the BBMV precipitate

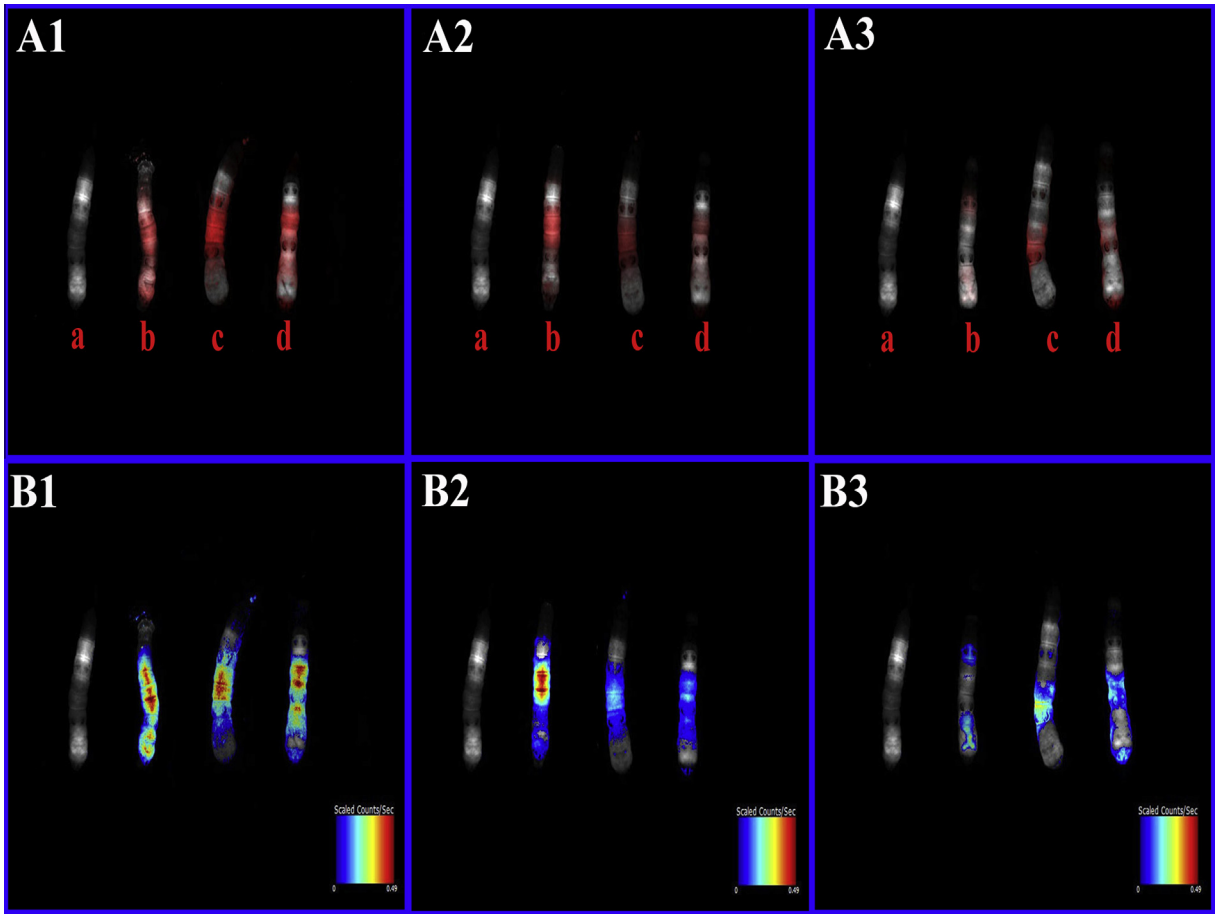

Fig.5. *In vivo* NIR fluorescence imaging of the silkworm targeting of the (images a) control, (images b) QD, (images c) Cry1Aa–QD, and (images d) Cry1Ac–QD probes. Spectrally unmixed in vivo fluorescence images of the silkworms at (1) 10 min, (2) 1 h, and (3) 3 h after being fed the probes are shown. The upper images (A1–A4) show the distribution of the red fluorescent signal from probes and the lower images (B1–B4) show the distribution of fluorescence intensity from the probes. The autofluorescence of the silkworms was removed by spectral unmixing of the images.

was suspended in 100 μl of the buffer and sonicated for 30 s on ice. The fluorescence of QDs bound to BBMVs was examined under a fluorescence microscope.

In vivo fluorescence imaging of silkworm

One-day-old third-instar silkworms were fed a 20-μl dose of probe per os (after 3 days without any food, a 20-μl drop of probe solution was placed on a mulberry leaf and the silkworm was forced to eat all the probe solution) and then placed in a petri dish containing fresh mulberry leaves. At various time points (10 min, 1 h, 3 h) after the silkworms were fed the probe, the silkworms were anesthetized by approximately 20 s exposure to diethyl ether and fluorescence images of the silkworms were acquired using an In Vivo imaging system.

Preparation and analysis of frozen sections

The frozen sections of the silkworms were prepared from 1-day-old fifth-instar silkworms. At various times (10 min, 1 h, 3 h) after treatment with 20 μl QD, Cry1Aa–QD, or Cry1Ac–QD probes for the experimental group and without any treatment for the control group, these silkworms were separately put into liquid nitrogen for about 30 s and then sectioned at 10 μm under a freezing microtome. The prepared sections were quickly observed and imaged using a fluorescence microscope.

Results and discussions

The prepared NIR CdTe/CdS QDs showed typical broad absorption spectra and narrow PL spectra with an emission peak at 702 nm (Fig. 2A). The TEM image revealed that the NIR-emitting QDs were spherical particles with good monodispersibility (Fig. 2B). As we all know, the photostability and cytotoxicity of fluorescent probes are critically important for biological applications. Owing to the pH of the alkaline midgut juice (10.0–11.0) [34,35], the purified QDs were dispersed in Na_2CO_3 buffer (pH 10.0) solution for in vitro and in vivo studies. As shown in Fig. 3A, it was found that QDs in Na_2CO_3 buffer (pH 10.0) solution had a good photostability (loss of PL <5%), which was much higher than that in PBS (pH 7.4) after 180 min excitation with 380-nm UV irradiation. Also, there was no agglomeration or any precipitation after storing at 4 °C for more than 3 months (see Fig. 3A, images a and b). Prior to embarking on the imaging studies on silkworm, we investigated the cytotoxicity effects of CdTe/CdS QDs on HeLa cells using different concentrations. As shown in Fig. 3B, the HeLa cell line maintained greater than 80% cell viability even after 24 h of treatment with QDs at concentration as high as 25 μg/ml, and HeLa cells exhibited no obvious morphological changes at various concentrations (from 0.25 to 25 μg/ml; Supplementary Fig. S1). The reason for the low cytotoxicity of QDs may be that the thick shell could prevent the release of free Cd^{2+} ions from the QD surface [36,37]. All of these results demonstrated that the superior photostability and low cytotoxicity of the

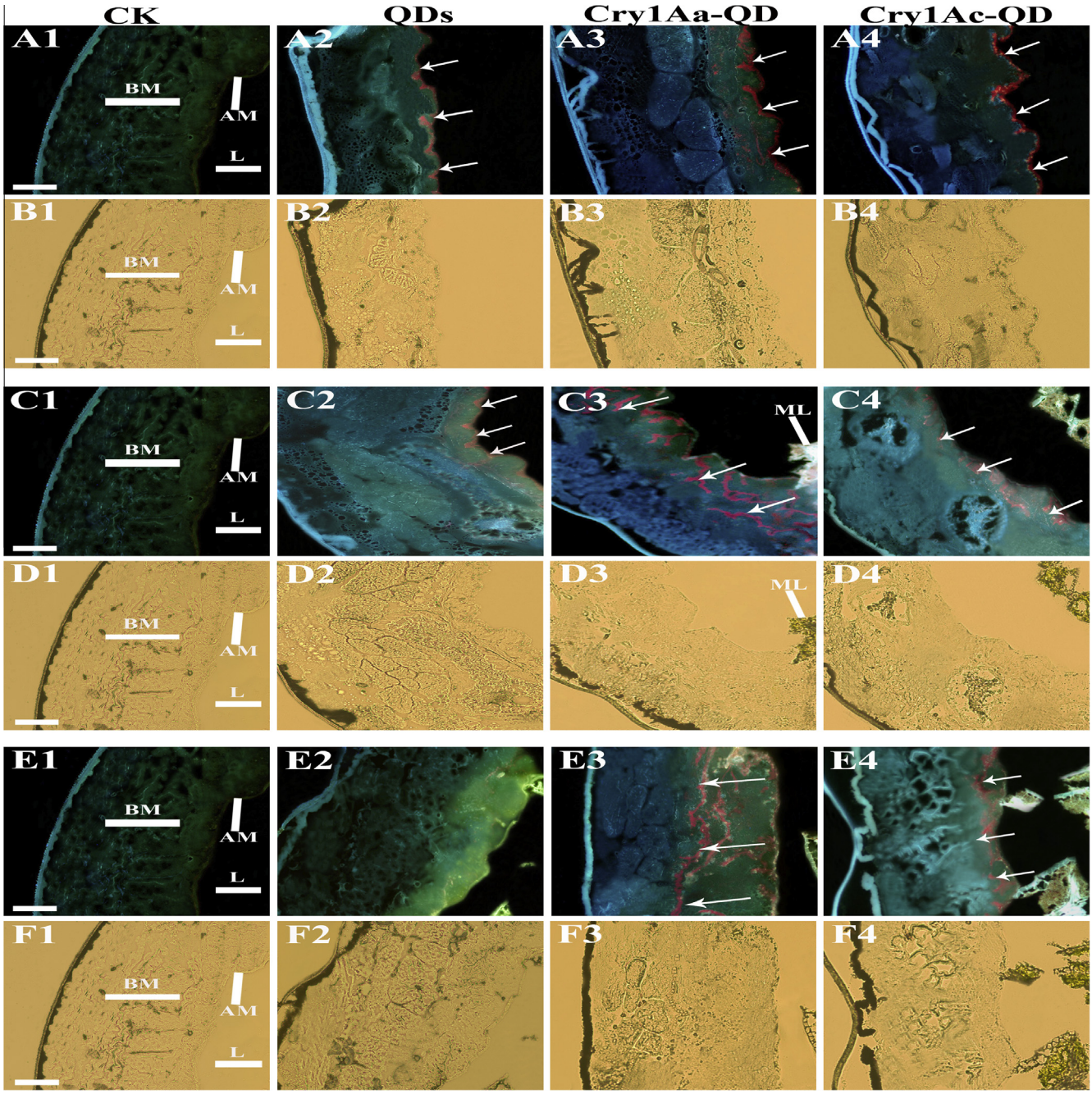

Fig.6. Fluorescence microscopic images of the frozen sections of the midgut tissue from silkworm. Transverse sections of untreated and QD-treated, Cry1Aa–QD probe-treated, and Cry1Ac–QD probe-treated worms after (A1–A4) 10 min, (C1–C4) 1 h, and (E1–E4) 3 h were observed in the dark field and (B1–B4, D1–D4, and F1–F4) in the bright field. Arrowheads indicate the probes' change in the midgut tissue. AM, apical membrane; BM, basement membrane; L, lumen; ML, mulberry leaves. Bars, 200 μm.

NIR QDs made their use for long-term and real-time bioimaging applications possible.

To use these photostable and biocompatible QDs as targeted biological probes, we conjugated Cry1Aa, Cry1Ac, and BSA proteins with QD 702 to produce Cry1Aa–QD, Cry1Ac–QD, and BSA–QD conjugates by the EDC/NHS conjugation strategy. The coupling effect, particle size analysis, and fluorescence performance of the protein–QD probes before and after coupling were characterized. As shown in Fig. 3C, the electrophoretic velocity of protein–QD conjugates was obviously lower than that of QDs, which confirmed that Cry1Aa, Cry1Ac, and BSA molecules were successfully introduced onto the surface of QDs. The reason for that was mainly due to the Cry1Aa, Cry1Ac, and BSA proteins increasing the molecular weight of the QDs and changing their charge density [38], thereby hindering the movement of the conjugates on the gel plate. The results of DLS (Fig. 3D) and PL spectra (Supplementary Fig. S2) also showed the successful coupling between the QDs and the proteins. Importantly, the size-distribution histogram (Supplementary Fig. S3) showed that the average sizes of the as-prepared NIR QDs and QD-labeled conjugates were all less than 20 nm. In this size range, the probes could get through the silkworm peritrophic membrane (a layer of film secreted by midgut epidermal cells; aperture is in the range of 20–30 nm) [39,40]. These results highly indicated the potential of QD-labeled conjugates for *in vivo* imaging.

To evaluate the specific binding of Cry1Aa–QD and Cry1Ac–QD probes, the extracted BBMVs were incubated with QDs, Cry1Aa–QD, Cry1Ac–QD, and BSA–QD conjugates. Fluorescence images of

the BBMVs were compared. As illustrated in Fig. 4, Cry1Aa–QD (Fig. 4A1 and B1) and Cry1Ac–QD (Fig. 4A2 and B2) probes both exhibited strong red fluorescent signal, but the Cry1Aa–QD probes binding to BBMVs showed higher fluorescence than Cry1Ac–QD, which implied that more Cry1Aa–QD probes specifically bound to BBMVs than Cry1Ac–QD. Meanwhile, the control studies using BSA–QD probes (Fig. 4A3 and B3) and QDs (Fig. 4A4 and B4) indicated that the amounts of QDs and BSA–QDs binding to BBMVs were very limited. These results confirmed that the Cry1Aa–QD and Cry1Ac–QD conjugates still retained the binding activity and specificity of Cry1Aa and Cry1Ac to midgut tissue.

There have been many reports using extracted proteins and tissues for probing the mode of action of Bt toxin binding *in vitro* [5,13–20]. However, the acquired results would probably deviate from the intact information. Here, a QD-based NIR fluorescence imaging method was used to directly and dynamically track the specific binding of CrylAa and CrylAc to the midgut tissue of the silkworm. The probes in living silkworms were monitored by measuring real-time *in vivo* NIR images to achieve intact tracking information of CrylAa and CrylAc binding at multiple time points (10 min, 1 h, 3 h). Fig. 5 shows the red fluorescent signals and the change in fluorescence intensity distribution of these probes in the midgut region during 3 h. As seen from Fig. 5A1–A3, the strong red fluorescent signals were all over the silkworm body 10 min after feeding the probes. One hour later, the red fluorescent signals principally concentrated in the midgut parts of the silkworm, as expected, but there were still many QDs, as a control group stayed in the midgut parts. That was probably due to the low ability to clean QDs totally from the living silkworm in a short time. However, after 3 h, it was apparent that there was almost no QD fluorescent signal in the midgut parts, but Cry1Aa–QD and Cry1Ac–QD probes almost absolutely rested on the midgut region. And the Cry1Aa–QD showed much stronger retention than the Cry1Ac–QD. Meanwhile, the fluorescent signals of the probes from silkworms were consistent with a characteristic about 704 nm peak of the Cry1Aa–QD and Cry1Ac–QD probes and were obviously different from the autofluorescence (Supplementary Fig. S4).

The silkworm models exhibited very strong fluorescent signals in the midgut part, which indicated that the Cry1Aa–QD and Cry1Ac–QD probes could target and home to midgut tissue within 3 h. Furthermore, the distribution of the fluorescent signal intensity of probes targeting *in vivo* was similar to that of probes binding to BBMVs *in vitro*, which further confirmed that Cry1Aa had more binding to midgut than Cry1Ac. The results of *in vivo* imaging raised a new approach for tracing the specific binding of Bt toxins *in vivo*. The QD-based NIR *in vivo* imaging technique for living silkworms has several outstanding advantages: (1) compared with the protein or BBMV extraction by detergent, it is scatheless for identification of target biomolecules; (2) this technique is also visual and allows us to observe clearly the real-time midgut targeting process of Cry1Aa and Cry1Ac without any extraction procedure. Furthermore, the ability to exclude interference from autofluorescence gives our method considerable ability to take a full view of how the action modes of Bt toxins affect their insecticidal activity.

To further investigate the specific labeling of Cry1Aa and Cry1Ac binding sites by the Cry1Aa–QD and Cry1Ac–QD probes, fluorescence images of the midgut sections of silkworms were compared, and strong red fluorescent signal was observed on the midgut sections. As shown in Fig. 6, red signal represents the probes' targeted sites, and the white arrows point out the targeted regions of the probes. As seen from the characteristic red fluorescence of the probes, it was observed that the probes first located on the apical membrane region (Fig. 6A1–A4). After an hour, most of the QDs as a control group still rested on the apical membrane region, while some Cry1Aa–QD and Cry1Ac–QD probes had transferred from the apical membrane areas to the basolateral regions (Fig. 6C1–C4). Fig. 6F1–F4 show the distribution of probes after 3 h. It was seen that there was little red signal from QDs in the midgut tissue, indicating the complete clearance of QDs by the excretory system. Meanwhile, it was found that the red fluorescent signals of CrylAa–QD probes were broader than those of CrylAc–QD in the midgut tissue (Fig. 6F1–F4). The results show that Cry1Aa, CrylAc binding sites are distributed mainly over the apical region and basolateral regions of the midgut tissue, whereas CrylAa binding sites are spread more widely. The wide range of binding targets observed for CrylAa suggests that CrylAa has a special structure capable of recognizing a ubiquitous structure of various proteins. Relatively, the limited binding sites for CrylAc show that CrylAc toxin has recognition sites different from those of Cry1Aa. Thus, there is a possibility that the difference in the binding site for toxins could affect the insecticidal activity. These results further indicate that the labeled QD probes could provide a new approach to observe the process of Cry1Aa and Cry1Ac targeting and tracing *in vivo* and verify the different binding patterns of Cry1Aa and Cry1Ac to the silkworm midgut. The preliminary results shown here are very encouraging and on the basis of the proposed new method, further studies on the action mechanism of Bt toxins will be under way.

Conclusions

In this study, the real-time midgut targeting and imaging in living silkworm was first conducted using CrylA-conjugated QD probes. For the first time, we applied NIR fluorescence imaging *in vivo* to research the specific binding of CrylAa and CrylAc to the midgut tissue of silkworm. It turned out that the broader binding sites of CrylAa could cause the different insecticidal activities of CrylAa and CrylAc as seen by the fluorescence imaging of sections. Therefore, this scatheless and visual imaging technique would be able to visualize the effects of various membrane elements and promises to have great potential of becoming a valid tool for promoting the development of the molecular mechanism of insect resistance to Bt toxins. It is hoped that an increased understanding of the complex interplay between Cry toxins and their target organisms will maintain the insecticidal ability of Cry toxins. Simultaneously, the improvement of insecticidal activity will depend on the mapping of the specificity binding regions in the Cry toxins to some extent.

Acknowledgments

We gratefully acknowledge funding support for this research from the National Natural Science Foundation of China (21175051, 21375043), Fundamental Research Funds for the Central Universities (2012SC04, 2013SC17), and Natural Science Foundation of Hubei Province Innovation Team (2011CDA115).

Appendix A. Supplementary material

Supplementary data associated with this article can be found, in the online version, at http://dx.doi.org/10.1016/j.ab.2013.11.011.

References

[1] A. Bravo, S. Likitvivatanavong, S.S. Gill, M. Soberón, *Bacillus thuringiensis:* a story of a successful bioinsecticide, Insect Biochem. Mol. Biol. 41 (2011) 423–431.
[2] S.E. Naranjo, Impacts of Bt transgenic cotton on integrated pest management, J. Agric. Food Chem. 59 (2011) 5842–5851.
[3] H. Hofte, H.R. Whiteley, Insecticidal crystal proteins of *Bacillus thuringiensis*, Microbiol. Mol. Biol. Rev. 53 (1989) 242.
[4] S.S. Gill, E.A. Cowles, P.V. Pietrantonio, The mode of action of *Bacillus thuringiensis* endotoxins, Annu. Rev. Entomol. 37 (1992) 615–634.

[5] A. Bravo, S.S. Gill, M. Soberon, Mode of action of *Bacillus thuringiensis* Cry and Cyt toxins and their potential for insect control, Toxicon 49 (2007) 423–435.
[6] M. Soberon, L. Pardo, G.C. Munoz, J. Sanchez, I. Gomez, H. Porta, A. Bravo, Pore formation by Cry toxins, Adv. Exp. Med. Biol. 677 (2010) 127–142.
[7] M. Soberon, S.S. Gill, A. Bravo, Signaling versus punching hole: how do *Bacillus thuringiensis* toxins kill insect midgut cells?, Cell Mol. Life Sci. 66 (2009) 1337–1349.
[8] D.G. Heckel, L.J. Gahan, S.W. Baxter, J.Z. Zhao, A.M. Shelton, F. Gould, B.E. Tabashnik, The diversity of Bt resistance genes in species of Lepidoptera, J. Invertebr. Pathol. 95 (2007) 192–197.
[9] G.P. Georghiou, A. Lagunes-Tejeda, The occurrence of resistance to pesticides in arthropods, Rome: Food and Agriculture Organization of the United Nations; 1991.
[10] E. Schnepf, N. Crickmore, J. Vanrie, D. Lereclus, J. Baum, J. Feitelson, D.R. Zeigler, D.H. Dean, *Bacillus thuringiensis* and its pesticidal crystal proteins, Microbiol. Mol. Biol. Rev. 62 (1998) 775–806.
[11] K. Van Frankenhuyzen, Insecticidal activity of *Bacillus thuringiensis* crystal proteins, J. Invertebr. Pathol. 101 (2009) 1–16.
[12] S. Tanaka, Y. Yoshizawa, R. Sato, Response of midgut epithelial cells to Cry1Aa is toxin-dependent and depends on the interplay between toxic action and the host apoptotic response, FEBS J. 279 (2012) 1071–1079.
[13] H. Hara, S. Atsumi, K. Yaoi, K. Nakanishia, S. Higurashi, N. Miura, H. Tabunoki, R. Sato, A cadherin-like protein functions as a receptor for *Bacillus thuringiensis* Cry1Aa and Cry1Ac toxins on midgut epithelial cells of *Bombyx mori* larvae, FEBS Lett. 538 (2003) 29–34.
[14] A. Shinkawa, K. Yaoi, T. Kadotani, M. Imamura, N. Koizumi, H. Iwahana, Binding of phylogenetically distant *Bacillus thuringiensis* Cry toxins to a *Bombyx mori* aminopeptidase N suggests importance of Cry toxin's conserved structure in receptor binding, Curr. Microbiol. 39 (1999) 14–20.
[15] K. Yaoi, K. Nakanishi, T. Kadotani, M. Imamura, N. Koizumi, H. Iwahana, R. Sato, *Bacillus thuringiensis* Cry1Aa toxin-binding region of *Bombyx mori* aminopeptidase N, FEBS Lett. 463 (1999) 221–224.
[16] C.R. Pigott, D.J. Ellar, Role of receptors in *Bacillus thuringiensis* crystal toxin activity, Microbiol. Mol. Biol. Rev. 71 (2007) 255–281.
[17] D.M. Hossain, T. Hayakawa, Y. Shitomi, K. Itoh, T. Mitsui, R. Sato, H. Hori, Histochemical analysis *of Bacillus thuringiensis* CrylA toxin binding to midgut epithelial cells of *Bombyx mori*, Pestic. Biochem. Physiol. 87 (2007) 30–38.
[18] H. Hara, S. Atsumi, K. Yaoi, K. Nakanishi, S. Higurashi, N. Miura, H. Tabunoki, R. Sato, A cadherin-like protein functions as a receptor for *Bacillus thuringiensis* Cry1Aa and Cry1Ac toxins on midgut epithelial cells of *Bombyx mori* larvae, FEBS Lett. 538 (2003) 29–34.
[19] M.K. Lee, R.E. Milne, A.Z. Ge, D.H. Dean, Location of a *Bombyx mori* receptor binding region on a *Bacillus thuringiensis* δ-endotoxin, J. Biol. Chem. 267 (1992) 3115–3121.
[20] P. Sharma, V. Nain, S. Lakhanpaul, P.A. Kumar, Binding of *Bacillus thuringiensis* Cry1A toxins with brush border membrane vesicles of maize stem borer (*Chilo partellus* Swinhoe), J. Invertebr. Pathol. 106 (2011) 333–335.
[21] M. Higuchi, K. Haginoya, T. Yamazaki, K. Miyamoto, T. Katagiri, K. Tomimoto, Y. Shitomi, T. Hayakawa, R. Sato, H. Hori, Binding of *Bacillus thuringiensis* Cry1A toxins to brush border membrane vesicles of midgut from Cry1Ac susceptible and resistant *Plutella xylostella*, Comp. Biochem. Physiol. 147 (2007) 716–724.
[22] J.L. Jurat-Fuentes, M.J. Adang, Importance of Cry1 d-endotoxin domain II loops for binding specificity in *Heliothis virescens*, Appl. Environ. Microbiol. 67 (2001) 323–329.
[23] L. Masson, L.J. Lu, A. Mazza, R. Brousseau, M.J. Adang, The CrylA(c) receptor purified from *Manduca sexta* displays multiple specificities, J. Biol. Chem. 270 (1995) 20309–20315.
[24] G. Hua, L. Masson, J.L. Jurat-Fuentes, G. Schwab, M.J. Adang, Binding analyses of *Bacillus thuringiensis* Cry d-endotoxins using brush border membrane vesicles of *Ostrinia nubilalis*, Appl. Environ. Microbiol. 67 (2001) 872–879.
[25] X. Zhang, K. Tiewsiri, W. Kain, L. Huang, P. Wang, Resistance of *Trichoplusia ni* to *Bacillus thuringiensis* toxin Cry1Ac is independent of alteration of the cadherin-like receptor for Cry toxins, PLoS One 7 (2012) 35991.
[26] D. Shao, Q.H. Zeng, Z. Fan, J. Li, M. Zhang, Y.L. Zhang, O. Li, X.G. Kong, H. Zhang, Monitoring HSV-TK/ganciclovir cancer suicide gene therapy using CdTe/CdS core/shell quantum dots, Biomaterials 33 (2012) 4336–4344.
[27] L.N. Chen, J. Wang, W.T. Li, H.Y. Han, Aqueous one-pot synthesis of bright and ultrasmall CdTe/CdS near-infrared-emitting quantum dots and their application for tumor targeting *in vivo*, Chem. Commun. 48 (2012) 4971–4973.
[28] X. Michalet, F.F. Pinaud, L.A. Bentolila, J.M. Tsay, S. Doose, J.J. Li, G. Sundaresan, A.M. Wu, S.S. Gambhir, S. Weiss, Quantum dots for live cells, in vivo imaging, and diagnostics, Science 307 (2005) 538–544.
[29] Y. He, Y.L. Zhong, Y.Y. Su, Y.M. Lu, Z.Y. Jiang, F. Peng, T.T. Xu, S. Su, Q. Huang, C.H. Fan, S.T. Lee, Water-dispersed near-infrared-emitting quantum dots of ultrasmall sizes for *in vitro* and *in vivo* imaging, Angew. Chem. Int. Ed. 50 (2011) 5695–5698.
[30] J. Wang, H.Y. Han, X.C. Jiang, L. Huang, L.N. Chen, N. Li, Quantum dot-based near-infrared electrochemiluminescent immunosensor with gold nanoparticle–graphene nanosheet hybrids and silica nanospheres double-assisted signal amplification, Anal. Chem. 84 (2012) 4893–4899.
[31] L. Niu, Y. Li, X.J. Li, X. Gao, X.G. Su, Study of the cytotoxicity of different kinds of water-soluble nanoparticles in human osteoblast-like MG-63 cells, Mater. Res. Bull. 12 (2012) 3654–3659.
[32] M. Wolfersberger, P. Luethy, A. Maurer, P. Parenti, F.V. Sacchi, B. Giordana, Preparation and partial characterization of amino acid transporting brush border membrane vesicles from the larval midgut of the cabbage butterfly (*Pieris brassicae*), Comp. Biochem. Physiol. 86 (1987) 301–308.
[33] M.D. Hossain, Y. Shitomi, Y. Nanjo, D. Takano, T. Nishiumi, T. Hayakawa, T. Mitsui, R. Sato, H. Hori, Localization of a novel 252-kDa plasma membrane protein that binds Cry1A toxins in the midgut epithelia of *Bombyx mori*, Appl. Entomol. Zool. 40 (2005) 125–135.
[34] H. Nakazawa, E. Tsuneishi, K.M. Ponnuvel, S. Furukawa, A. Asaoka, H. Tanaka, J. Ishibashi, M. Yamakawa, Antiviral activity of a serine protease from the digestive juice of *Bombyx mori* larvae against nucleopolyhedrovirus, Virology 321 (2004) 154–162.
[35] L.M. Field, A.A. James, E. Kotani, T. Niwa, M. Tokizane, K. Suga, Y. Sugimura, K. Oda, H. Mori, T. Furusawa, Cloning and sequence of a cDNA for a highly basic protease from the digestive juice of the silkworm, *Bombyx mori*, Insect Mol. Biol. 8 (1999) 299–304.
[36] Y.Y. Su, M. Hu, C.H. Fan, Y. He, N.Q. Li, W.X. Li, L.H. Wang, P.P. Shen, Q. Huang, The cytotoxicity of CdTe quantum dots and the relative contributions from released cadmium ions and nanoparticle properties, Biomaterials 31 (2010) 4829–4834.
[37] B. Tang, L.H. Cao, K.H. Xu, L.H. Zhuo, J.C. Ge, Q.L. Li, Y.J. Yu, A new nanobiosensor for glucose with high sensitivity and selectivity in serum based on fluorescence resonance energy transfer (FRET) between CdTe quantum dots and Au nanoparticles, Chem. Eur. J. 14 (2008) 3637–3644.
[38] K.E. Sapsford, K.M. Tyner, B.J. Dair, J.R. Deschamps, I.L. Medintz, Analyzing nanomaterial bioconjugates: a review of current and emerging purification and characterization techniques, Anal. Chem. 83 (2011) 4453–4488.
[39] R.V. Barbehenn, M.M. Martin, Peritrophic envelope permeability in herbivorous insects, J. Insect. Physiol. 41 (1995) 303–311.
[40] L. Fiandra, M. Casartelli, G. Cermenati, N. Burlini, B. Giordana, The intestinal barrier in lepidopteran larvae: permeability of the peritrophic membrane and of the midgut epithelium to two biologically active peptides, J. Insect Physiol. 55 (2009) 10–18.